Effective slice thickness in limited-angle tomography

Seungjun Yoo[a], Minsoo Ryoo[a], Jinwoo Kim[b] and Ho Kyung Kim [a,b,*]
[a] *School of Mechanical Engineering, Pusan Nat'l Univ., Busandaehakro 63beon-gil, Busan 46241*
[b] *Center for Advanced Medical Engineering Research, Pusan Nat'l Univ., Busandaehakro 63beon-gil, Busan 46241*
[*] *Corresponding author: hokyung@pusan.ac.kr*

1. Introduction

Limited-angle tomography (LAT) is an x-ray imaging technique for reconstructing a three-dimensional image based on sparse projection data. The LAT is generally used for industrial non-destructive testing on thin slab geometry such as printed circuit boards (PCBs) which have a large difference of thicknesses with respect to the projection angle [1,2]. The conventional filtered backprojection (FBP) algorithm is one of the most widely used methods for LAT, but the FBP-based LAT suffers from artifacts in reconstructed images since the sparse projection data results in the null space of the Fourier domain [3]. These artifacts limit spatial resolution along the depth direction. The artifacts can be reduced by additional filtering but linear filtering is not sufficient to recover the missing Fourier data. As an alternative for linear filtering, low-resolution cross-sectional images can be obtained by truncating Fourier data.

Since it is difficult to compensate for the uncollected data, we propose a theoretical model describing the effective slice thickness for FBP-based LAT, which is the maximum thickness that can be properly reconstructed, with respect to the scan ranges. From effective slice thickness, we define slice thickness (i.e., z-directional voxel pitch) and the proposed method is validated by evaluating artifact-spread function (ASF) and its half-width at half-maximum (HWHM) using aluminum disc phantom.

2. Methods and Materials

2.1 Theoretical background

For the FBP-based LAT algorithm, a single slice $f(x,y)$ at a specific depth z can be obtained as:

$$f(x,y;z) = k\int_{\beta_{\text{scan}}} \frac{D^2}{(d-l)^2} g_\beta^*(u,v)\,\mathrm{d}\beta, \quad (1)$$

where β_{scan} is the total scan angle, $g_\beta^*(u,v)$ is the filtered projection data, and k refers to the normalization factor. D and d respectively denote the source-to-axis of rotation (AOR) and source-to-detector distance, and l is the distance between reconstructed voxels and AOR.

The filtered projection data $g_\beta^*(u,v)$ can be obtained by integrating the convolution of the weighted projection data and the filter h.

$$g_\beta^*(u,v) = \int_{-\infty}^{\infty}\left[\frac{D^2}{\sqrt{D^2+u^2+v^2}} g_\beta(u,v)\right] h\left(\frac{Dx'}{d-l}-u\right)\mathrm{d}\beta, \quad (2)$$

where x' indicates the x-axis rotated by the projection angle β.

The impulse response of LAT can be approximated as $(\beta_{\text{scan}}|f_u|)^{-1}$ [4] and filter H in the frequency domain is

$$H(f_u) = \beta_{\text{scan}}|f_u|W(f_u). \quad (3)$$

It is a typical ramp filter scaled by β_{scan} and an additional window function, called the spectral filter [5], is adjusted to regularized high-frequency noise. Then we adapt Hann window as a window function:

$$W(f_u) = \frac{1}{2}\left[1+\cos\left(\frac{\pi f_u}{B_{f_u}}\right)\right] \text{ for } |f_u| < B_{f_u}, \quad (4)$$

where B_{f_u} is the cutoff frequency, which is determined as the Nyquist frequency of the detector pixel pitch p.

The voxel size of the LAT depends on the magnification $M = d/D$ and β_{scan}. Based on the parallel-beam geometry, the reconstructed volume can be represented as a cylinder with a radius r, and the distance between the maximum and minimum points where the incident beam is tangent can be defined as the reconstructable depth. We define this depth as the effective slice thickness:

$$d_{eff} = 2r\sin(\beta_{\text{scan}}/2) \quad (\beta_{\text{scan}} \le 180^\circ). \quad (5)$$

Eq. (5) shows that the reconstructable depth gradually decreases with decreasing β_{scan} and more voxels are required to express the same depth compared to conventional cone-beam computed tomography (CBCT) geometry. Therefore, the slice thickness Δz for LAT reconstruction can be defined as:

$$\Delta z = \left(\frac{p}{M}\right)/\sin(\beta_{\text{scan}}/2). \quad (6)$$

2.2 Validation

To validate the theoretical model, the ASF and its HWHM are evaluated by experiments and numerical simulations for an aluminum disc phantom. The ASF(z) can be defined as a ratio of contrasts of the aluminum disc at a central slice (z=0) and other slices.

$$\text{ASF}(z) = \frac{\Delta\mu(z)}{\Delta\mu(z)|_{z=0}}, \quad (7)$$

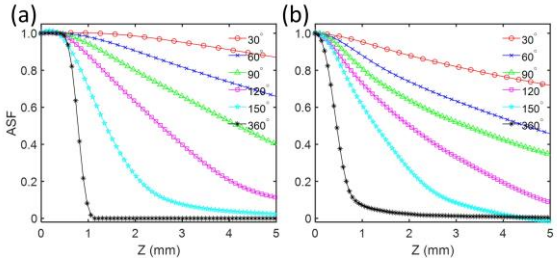

Fig. 1. ASF curves obtained for various β_{scan}. (a) and (b) represent numerical simulation and experimental results, respectively.

where $\Delta\mu(z)$ denotes the contrast of the aluminum disc.

The phantom is composed of a cylindrical polymethyl methacrylate which has a diameter of 30 mm and a height of 30 mm, and an embedded aluminum disc with a diameter of 10 mm and a thickness of 1 mm. For the numerical simulations, the phantom is generated with a dimension of 512 × 512 × 512 and a voxel pitch of 0.1 mm.

Projection data for various β_{scan} are acquired using a bench-top CBCT system. A tungsten target x-ray tube (XTF5011, Oxford Instruments, Oxfordshire, UK) emits a 45 kVp spectrum at each step angle of $\Delta\beta$ = 1°, and a 1032 × 1548 formatted x-ray detector (Shad-o-Box 1548 HS, Teledyne Rad-icon Imaging Corp., Sunnyvale, CA) with a pixel pitch of 99 μm is used for image acquisition. D and d are 665.86 mm and 443.91 mm, respectively. The numerical simulations for the same condition described above are performed using MATLAB® (R2020b, MathWorks, Natick, MA). In addition, the same experiments for a PCB sample are performed to provide qualitative analysis for more practical objects.

3. Preliminary Results

Fig. 1 compares the ASF curves obtained for various β_{scan}. The artifacts due to the sparse projection become severe as β_{scan} decreases. The HWHMs of ASFs for various β_{scan} are summarized in Fig. 2. Lines in Fig. 2 are estimated HWHM curves by $a/\sin(\beta_{\text{scan}}/2) + b$, which is based on our effective slice thickness model.

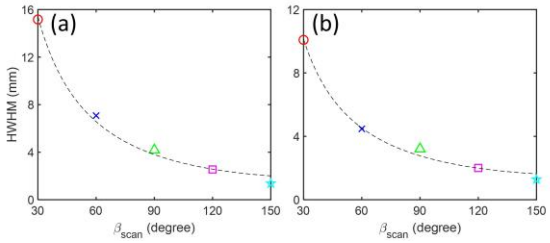

Fig. 2. Summary of HWHM values calculated from ASFs shown in Fig. 1. (a) and (b) represent numerical simulation and experimental results, respectively.

The model describes well the simulation and experimental results.

Fig. 3 compares tomographic images of a PCB sample that are reconstructed using anisotropic voxels that account for effective slice thickness and conventional isotropic voxels. As shown in Fig. 3(a), visual inspection validates that the effective slice thickness increases with increasing β_{scan}. In contrast, the reconstruction with isotropic voxel size results in significant blurring along the z-direction.

4. Conclusion

A theoretical model for describing effective slice thickness for the FBP-based LAT algorithm has been introduced. The proposed model showed good agreement with simulation and experimental results for a wide range of β_{scan}. Qualitative analysis for the PCB sample showed a large improvement in image quality compared to the conventional method, despite the incomplete reconstruction due to the lack of data is inevitable. The modeling and validation of the effective slice thickness for the cone-beam geometry will be our next study.

ACKNOWLEDGEMENTS

This work was supported by the National Research Foundation of Korea (NRF) grant funded by the Korea government (MSIP) (No. 2021R1A2C1010161).

REFERENCES

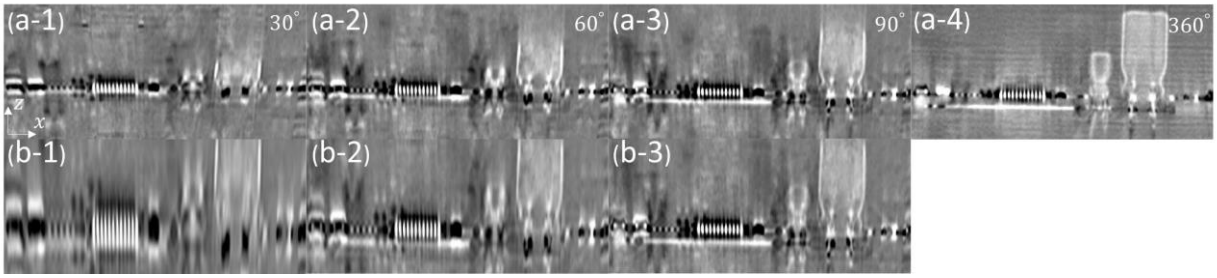

Fig. 3. Comparison of coronal sections of a PCB sample. The top and bottom rows show the reconstruction results using effective slice thickness and isotropic voxel, respectively. Columns from left to right respectively represent β_{scan} of 30, 60, 90, and 360 degrees.

[1] M. K. Cho, H. Youn, S. Y. Jang, and H. K. Kim, Cone-Beam Digital Tomosynthesis for Thin Slab Objects, NDT&E International, Vol. 47, pp. 171-176, 2012.
[2] N. S. O'Brien, R. P. Boardman, I. Sinclair, and T. Blumensath, Recent Advances in X-Ray Cone-Beam Computed Laminography, Journal of X-Ray Science and Technology, Vol. 24, No. 5, pp. 691-707, 2016.
[3] D. Kim, D. W. Kim, J. Yon, S. Ha, S. H. Kim, H. Youn, and H. K. Kim, Spatial Resolution and Blurring Artifacts in Digital X-Ray Tomosynthesis, IEEE Transactions on Nuclear Science, Vol. 65, No.5, pp. 1180-1186, 2018.
[4] T. Mertelmeier, J. Orman, W. Haerer, and M. K. Dudam, Optimizing filtered backprojection reconstruction for a breast tomosynthesis prototype device, Proceedings of Medical Imaging, Physics of Medical Imaging, SPIE, Vol. 6142, pp. 131-142, 2006.
[5] G. Lauritsch and W. H. Härer, Theoretical Framework for Filtered Backprojection in Tomosynthesis, Proceedings of Medical Imaging, Image Processing, SPIE, Vol. 3338, pp. 1127-1137, 1998.